ARTICLE NO. 78-237

Acoustic Suppression in a Pulsed Chemical Laser

Darrell R. Ausherman,* Irwin E. Alber,† and Eric Baum†
TRW Defense and Space Systems Group, Redondo Beach, Calif.

The analytical and experimental studies aimed at developing an acoustic attenuator for a high-energy pulsed chemical laser are described. A numerical finite-difference code was developed to analyze the attenuation of strong pressure waves (shocks) in ducts. The attenuation concepts analyzed include variable flow area, vented walls, porous flow-through absorbers, and combinations of these. Experimental results were obtained for a vented duct attenuator on a shock tube. The code was used to design the acoustic attenuator of a 50-pulse/s D_2/F_2 laser module. Code predictions for the laser device were compared with experimental data.

Nomenclature

A = cross-sectional area
a = vent area per unit duct length
C_D = discharge coefficient
C_v = specific heat at constant volume
e = specific internal energy
f = drag force per unit volume of a fluid acting on a porous media
$\hat{i}$ = unit vector parallel to duct centerline pointing in the $+x$ direction
M = Mach number
P = pressure
q = heat transfer per unit volume from fluid to porous media
R = gas constant
S_i = source-sink terms of mass, momentum, and energy
t = time
T = temperature
u_s = velocity of fluid leaving the duct
u = velocity of fluid in the duct
x = distance along the duct
α = vent area per unit duct volume
γ = ratio of specific heats
ρ = density
σ = mass entering the duct per unit length per unit time

Subscripts

a = ambient conditions
s = fluid conditions entering or leaving duct
sy = components perpendicular to duct centerline
sx = component parallel to duct centerline

I. Introduction

In repetitively pulsed D_2/F_2 high-energy chemical lasers, large pressure disturbances are generated in the laser cavity by the laser initiation process. If these pressure disturbances, which are created each time the laser is fired, are not rapidly attenuated, regions with nonuniform density will be produced. These nonuniform regions can result in poor beam quality.

There are two ways in which pressure disturbances can produce inhomogeneous regions in the lasing gas. In the most direct way, pressure disturbances that are present when the laser is fired result in density disturbances due to the compressibility of the gas. In a less direct way, pressure disturbances which are present during the injection of the fuel slug can also result in density nonuniformities in the fuel slug. Pressure fluctuations during the injection of fuel result in entropy variations in the fuel slug because the injection process is nonisentropic (choked orifice plates are most frequently used). These entropy variations will result in density variations in the fuel slug even if pressure disturbances are completely damped out by the time the fuel slug has flowed into the laser cavity. Thus, the pressure disturbances created by a laser pulse must be damped out to acoustic levels ($\Delta P/P < 10^{-3}$) by the time the fuel for the next pulse is being injected into the device. As a rule of thumb, the pressure wave suppression time is approximately one-third the pulse repetition period.

This paper describes recent analytical and experimental studies aimed at developing an acoustic attenuator capable of meeting the stringent requirements of a high-energy pulsed laser system. To treat all of the nonlinear wave interaction processes associated with pulsed chemical lasers properly, a numerical finite-difference code (called FACTS) was developed to solve the quasi-one-dimensional time-dependent equations of motion. Appropriate sources in the model were included to describe 1) a continuous purge and fuel gas flow, 2) gas flow through a porous medium, and 3) inflow and outflow of gas through vents in the side walls of the duct.

The FACTS code was used to design the acoustic attenuator for an experimental device which was built to study the flameout characteristics of a 50-pulse/s D_2/F_2 laser system. A comparison was made between predicted and measured pressure time histories for this device.

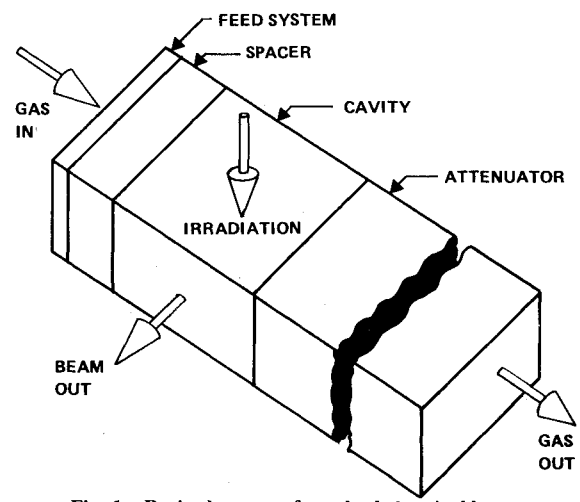

Fig. 1 Basic elements of a pulsed chemical laser.

Presented as Paper 78-237 at the AIAA 16th Aerospace Sciences Meeting, Huntsville, Ala., Jan. 16-18, 1978; submitted Aug. 7, 1978; revision received Jan. 12, 1979.

Index categories: Lasers; Shock Waves and Detonations; Aeroacoustics.

*Member Technical Staff, Vulnerability and Hardness Laboratory. Member AIAA.

†Member Technical Staff, Engineering Sciences Laboratory.

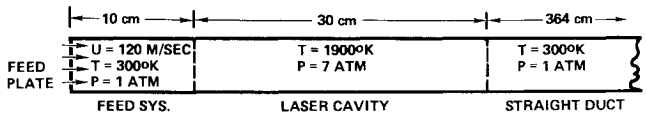

Fig. 2 Schematic of one-dimensional flow channel and initial conditions for wave interaction calculations.

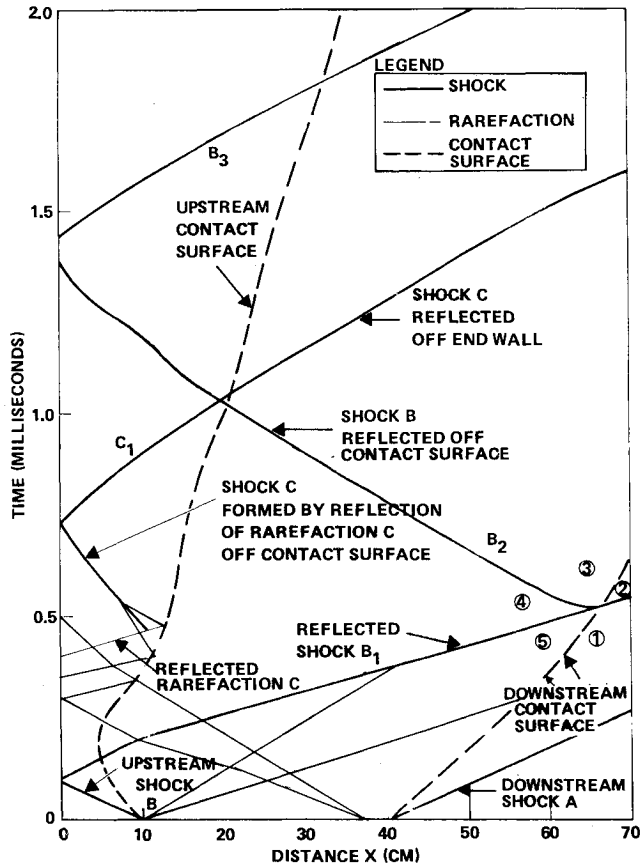

Fig. 3 *x-t* diagram of shock wave and rarefaction wave interactions in the laser cavity for the configuration shown in Fig. 2 with no attenuation in the downstream duct.

II. Physical Problem

The basic elements of a pulsed chemical laser are shown in Fig. 1. The feed system supplies an alternating flow of fuel and inert purge gas. When a slug of fuel is in the laser cavity, flashlamp irradiation ignites the fuel mixture, resulting in lasing. The inert purge gas located between the feed system and the cavity prevents the combustion process from propagating up into the feed system.

In repetitively pulsed D_2/F_2 chemical laser systems, large pressure and density disturbances are generated in the laser cavity by the heating of the laser gas caused by the very rapid heat release produced by the chemical reaction of the flashlamp-dissociated flourine with the pulsed D_2 fuel slug. The energy release process takes place in a short time, compared to acoustic travel times. It is completed within 10 to 100 μs after flashlamp initiation. The near-constant-volume initiation process thus leaves a reacted gas mixture filling the laser cavity, with temperatures on the order of 1900 K and pressures on the order of 7 atm. About one-half of the initial thermal translational energy after lasing will be transferred into shock, compression, and rarefaction wave motion; the remainder of the energy will remain in the form of residual gas heating. The residual high-temperature ($\sim$900 K) slug of gas is subsequently convected out of the system by the flowing purge gas.

Considerable insight into the problem of acoustic wave suppression can be obtained by observing the sequence of

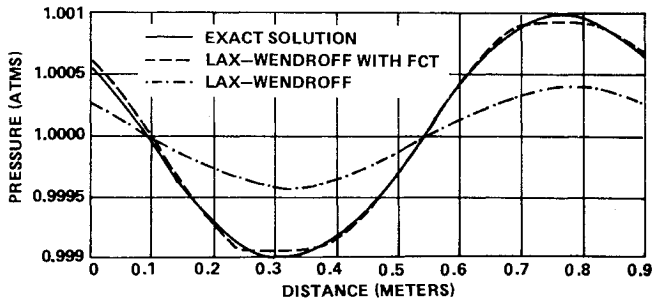

Fig. 4 Effects of numerical diffusion, pressure vs distance for a right running wave after 1000 timesteps or 7.4 wavelengths of travel.

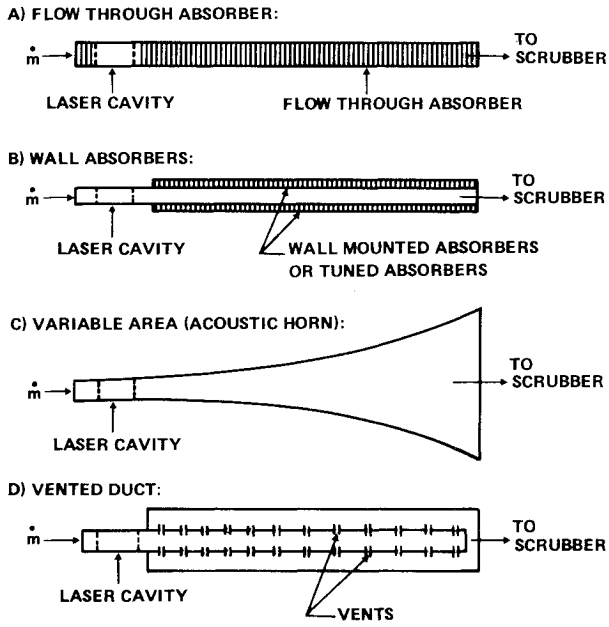

Fig. 5 Some of the attenuation concepts considered.

events during a single pulse of a laser device with no means of pressure wave attenuation. Such a device is shown in Fig. 2, where at time $t=0$, a high-pressure, high-temperature region is located between $x=10$ and $x=40$ cm downstream of the sonic orifice feedplate.

The early wave formation process is similar to that in a shock tube where two diaphragms burst simultaneously. This process is easily visualized with the aid of an *x-t* diagram. In an *x-t* diagram the trajectories of contact surfaces, shock waves, and rarefaction waves are plotted in an *x-t* coordinate system. An *x-t* wave diagram for this device is shown in Fig. 3.

Shock waves are sent upstream and downstream followed by the contact surfaces, which separate the shock-heated gas and the high-temperature driver gas. Expansion or rarefaction waves cross in the center of the lasing cavity. Reflections of the waves occur both off the upstream feed plate and off the contact surfaces. When shock or rarefaction waves pass through regions where the acoustic impedance changes rapidly (as it would at the contact surfaces illustrated in Fig. 3), the incident wave is transformed into a reflected and a transmitted wave. This interaction process quickly leads to the formation of a multitude of waves. Only the most significant waves are shown in the *x-t* diagram of Fig. 3. Of particular significance is the strength of the upstream reflected shock wave and its interaction with the edge of the downstream contact surface. This interaction causes a reflected shock wave to propagate back into the cavity in about 1.5 ms. Similar interactions can occur between the shock waves of a given pulse and the contact surfaces generated by the previous pulse.

III. Analysis

Approach

The attenuation process is dominated by the nonlinear one-dimensional aspects of the problem. The interactions among shock waves, rarefaction waves, hot/cold gas interfaces, and the attenuation elements of the device are the most important aspects of the attenuation process. The approach is to develop a model that would treat the nonlinear one-dimensional aspects of the problem. This model is then used to evaluate various attenuation concepts on the basis of their ability to attenuate the highly nonlinear shock and rarefaction waves that dominate the attenuation process.

Equations

The equations that describe the unsteady, one-dimensional flow of a gas in a duct of slowly varying cross-sectional area are:

Conservation of mass

$$\frac{\partial}{\partial t}(\rho A) = -\frac{\partial}{\partial x}(\rho A u) - S_1 \tag{1}$$

Conservation of momentum

$$\frac{\partial}{\partial t}(\rho A u) = -\frac{\partial}{\partial x}(\rho A u^2) - A\frac{\partial}{\partial x}(P) - S_2 \tag{2}$$

Conservation of energy

$$\frac{\partial}{\partial t}[\rho A(e+u^2/2)] = -\frac{\partial}{\partial x}[\rho A(e+u^2/2+P/\rho)u] - S_3 \tag{3}$$

Ideal gas equation of state

$$P=\rho RT=(\gamma-1)\rho e \tag{4}$$

and for a perfect gas

$$e=C_v T=[R/(\gamma-1)]T \tag{5}$$

S_1, S_2, and S_3 are source-sink terms with units of mass, momentum, and energy rates per unit length of duct, respectively. These source-sink terms are used to account for a perforated duct wall vented to the atmosphere and to account for sections of duct filled with a permeable sound absorbing material. In addition, these source-sink terms are used to model a sonic orifice plate mean flow inlet condition.

Source Terms

The general form of the source terms for wall venting is given by

$$S_1=\sigma \tag{6}$$

$$S_2=\sigma u_s \cdot \hat{i} \tag{7}$$

$$S_3=\sigma\left(e_s+\frac{P_s}{\rho_s}+\frac{|u_s|^2}{2}\right) \tag{8}$$

where σ is the mass flowing into the duct per unit length per unit time, and where the subscript s denotes conditions as the fluid enters or leaves the duct. This line source of mass σ can be expressed in general as

$$\sigma=C_D\rho_s u_s \cdot a_s \tag{9}$$

where a_s is a vector with magnitude equal to the vent area per unit length of the duct in an outward normal direction relative to the surface of the duct, and C_D is the discharge coefficient for the flow through the vents. In general, the vent area per unit length will have to be specified as a function of position in the duct. The condition of the fluid entering or leaving the duct will depend on the conditions inside and outside the duct and will have to be calculated.

The specific form of the source terms for the case of side wall venting will depend on the specific configuration of the vent holes and on the manifold collecting the vented gases. For the application considered here, it was assumed that the duct is venting to the atmosphere. Under these conditions, the properties of the fluid as it enters or leaves the duct were determined by assuming quasisteady compressible flow through a nozzle connecting the atmosphere with the flow in the duct. If the static pressure inside the duct is less than atmospheric, the flow will be into the duct and the inflow conditions are given by

$$M_s=\min\left[\left\{\left(\frac{2}{\gamma-1}\right)\left[\left(\frac{P_a}{P}\right)^{[(\gamma-1)/\gamma]}-1\right]\right\}^{1/2}, 1.0\right] \tag{10}$$

$$\rho_s=\rho_a\Big/\left(1+\frac{\gamma-1}{2}M_s^2\right)^{[1/(\gamma-1)]} \tag{11}$$

$$P_s=P_a\Big/\left(1+\frac{\gamma-1}{2}M_s^2\right)^{[\gamma/(\gamma-1)]} \tag{12}$$

$$e_s=P_s/[\rho_s(\gamma-1)] \tag{13}$$

$$u_{sy}=M_s\sqrt{\gamma P_s/\rho_s} \tag{14}$$

$$u_{sx}=0 \tag{15}$$

Equation (10) gives the Mach number of the fluid as it enters the duct and accounts for the fact that the flow may be choked as it enters the duct if the pressure ratio is high enough. Equations (11) and (12) are used to evaluate the density and pressure once the Mach number is known. The internal energy and the y component of the velocity are given by Eqs. (13) and (14). In this case, when the flow is into the duct, the x component of the velocity is zero as it enters the duct.

When the static pressure in the duct is greater than atmospheric pressure, the outflow conditions are given by

$$M_s=\min\left[\left\{\left(\frac{2}{\gamma-1}\right)\left[\left(\frac{P}{P_a}\right)^{[(\gamma-1)/\gamma]}-1\right]\right\}^{1/2}, 1.0\right] \tag{16}$$

$$\rho_s=\rho\Big/\left(1+\frac{\gamma-1}{2}M_s^2\right)^{[1/(\gamma-1)]} \tag{17}$$

$$P_s=P\Big/\left(1+\frac{\gamma-1}{2}M_s^2\right)^{[\gamma/(\gamma-1)]} \tag{18}$$

$$e_s=P_s/[\rho_s(\gamma-1)] \tag{19}$$

$$u_{sy}=M_s\sqrt{\gamma P_s/\rho_s} \tag{20}$$

$$u_{sx}=u \tag{21}$$

The source terms that take into account flow through a porous media are given by

$$S_1=0 \tag{22}$$

$$S_2=-fA \tag{23}$$

$$S_3=-qA \tag{24}$$

where f is the drag force per unit volume of the fluid on the porous media, and q is the heat transfer per unit volume from the fluid to the porous media. The drag force term can be

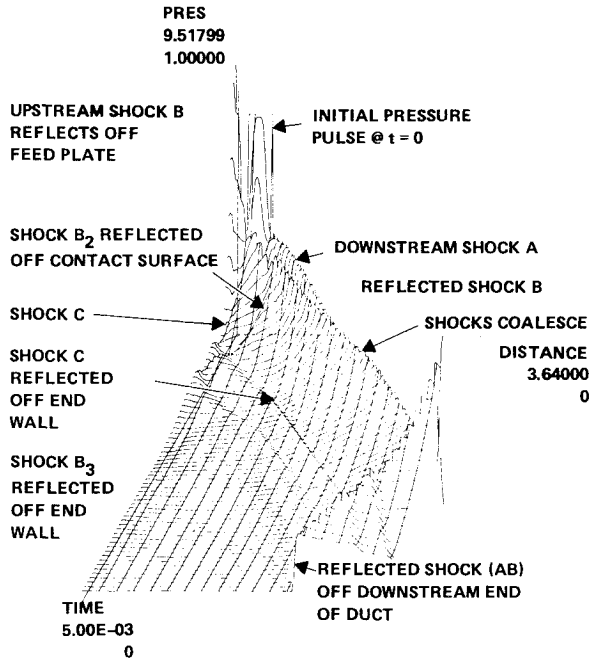

Fig. 6 Three-dimensional plot of pressure as a function of distance and time for the no attenuation case shown in Figs. 2 and 3.

modeled by using Darcy's law.[1] Once the drag force is specified, the heat transfer function can be determined by using Reynolds' analogy.[2]

Boundary Conditions

In the repetitively pulsed chemical laser design, fuel and purge flows are injected through choked orifice plates located at one end of the device. The cross-sectional area of the choked orifice plates is small relative to the total cross-sectional area. The orifice plate behaves primarily like a rigid wall when interacting with pressure or rarefaction waves in the duct. Thus, at the upstream boundary, fluid is injected at sonic velocity. Pressure waves are simultaneously reflected back as if the wall were a solid barrier. The downstream end of the laser device can be either fully closed or fully open to the exhaust manifold.

IV. Numerical Solution

A Lax-Wendroff differencing scheme with flux-corrected transport[3,4] (FCT) was used to generate the time-dependent solutions to Eqs. (1-3). The Lax-Wendroff differencing technique intentionally diffuses the solution in order to treat problems with strong gradients or shocks. The FCT technique is a method of removing the diffusion added to assure numerical stability. Shock waves that take five or six mesh spaces to describe with the Lax-Wendroff method alone are described in two mesh spaces when the FCT technique is used.

In the problem considered here, we were interested not only in the initial shock waves, but also in the whole attenuation process from the strongest shocks formed down to pressure waves 0.001 atm amplitude. To be sure that diffusion in the numerical method would not wipe out low-amplitude waves, a calculation of a low-amplitude pressure wave traveling to the right was made. A re-entrant boundary condition was used to minimize the number of nodes required for the calculation. With the re-entrant boundary condition, what goes out the downstream end of the mesh is fed into the upstream end of the mesh. This allowed us to calculate a right running wave with only one wavelength of zones. A sinusoidal pressure wave of amplitude 0.002 atm, propagating to the right into a gas with a sound speed of 553 m/s and a density of 0.507 g/m^3, was calculated using Lax-Wendroff differencing with and without FCT. The results are shown in Fig. 4 where

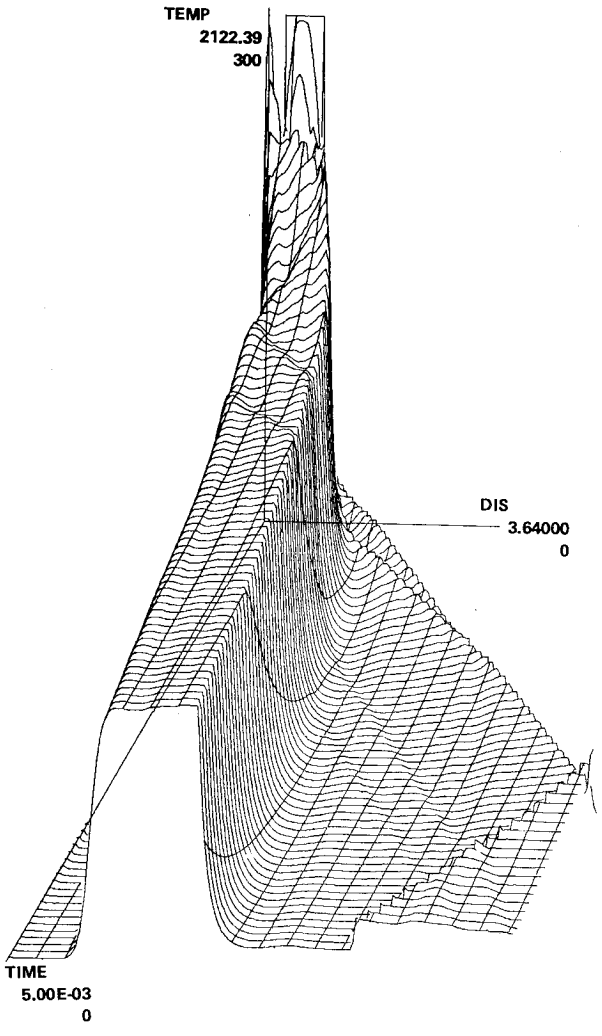

Fig. 7 Three-dimensional plot of temperature as a function of distance and time for the case of no attenuation shown in Figs. 2 and 3.

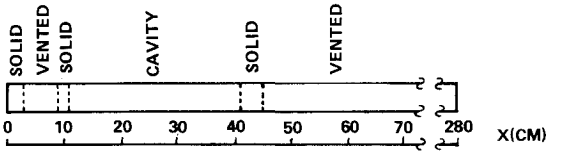

Fig. 8 Basic cavity and vented duct attenuator geometry including upstream venting.

pressure vs distance is plotted after 1000 cycles, which corresponds to a time of 12.05 ms when the wave had traveled 6.66 m or 7.4 wave-lengths. With Lax-Wendroff alone, the amplitude was 60% low by the time the wave had traveled 7 wavelengths. The addition of FCT reduced the amplitude error to less than 10%. With both methods the wave propagation speed was within a 0.001%. While FCT was developed primarily to improve calculations involving strong gradients or shocks, the sine wave results indicate that significant improvement was obtained for low-amplitude waves as well. In fact, without the reduced diffusion provided by FCT, the low amplitude pressure waves would be artifically smoothed out by the finite difference calculations.

The numerical treatment of the mean-flow/reflective-boundary condition at the device entrance posed an additional problem. The solution was to use the standard reflective boundary and inject the required amount of fluid with the correct momentum and energy into the node adjacent to the reflective wall. Two means of doing this were tried. The first method added the correct amount of mass, momentum, and

energy into the injection node from the wall after each time-step. The results were, in general, satisfactory, but a definite discontinuity at the injection node resulted. The second approach used a source-term method. The mass, momentum and energy were injected through the source terms, which were previously coded to handle venting, boundary layer, and heat transfer effects. The results were a much smoother and more realistic simulation of the injection process.

V. Results and Discussion

Evaluation of Attenuator Concepts

The FACTS code was used to investigate the following basic methods of acoustic suppression: a duct filled with a flow-through absorbing material; a duct lined with sound absorbing material; a variable area duct, e.g., acoustic horns (impedance matching); and a vented duct. Figure 5 illustrates schematically how some of these methods, either alone or in combination, can be used for pulsed chemical laser applications. The following discussion presents some of the evaluations we have made of the preceding attenuation methods, based on pressure histories calculated by the FACTS code.

A flow-through device (a constant-area duct packed with a fibrous acoustic absorbing medium) was found to have too large a pressure drop through the absorber. A similar design with perforated duct walls was found to reduce the pressure drop to an acceptable level. With suitable permeability of the absorber and adequate venting area, this concept could provide adequate attenuation. However, because of the material compatibility problem (finely divided absorbing medium in contact with hot fluorine and DF), this approach was tabled in favor of a further search for an attenuator without this materials problem.

An acoustic horn was also investigated, using a horn size and shape that would efficiently radiate a linear acoustic quarter-wave disturbance from the cavity. The horn proved to be a poor radiator of the nonlinear disturbance, as the pressure amplitude in the cavity remained large even after 10 ms. The failure of linear acoustics-based ideas, when used in the nonlinear regime, motivated our current design philosophy of starting with an attenuation scheme known to be effective for nonlinear waves and trying to extend its usefulness into the acoustics range, rather than vice versa.

Finally, the vented duct approach was investigated, since vented ducts are known to attenuate shock waves. A series of FACTS calculations showed that the vented duct attenuator gives excellent overall acoustic suppression. The best attenuation was found if one optimized the following parameters: vent area per unit duct volume (α), vented duct length, and length of the nonvented region. Most investigations of the vented duct concept were for a constant duct cross-sectional area and a constant vent area (α = constant). A few cases have been run with variable duct cross-sectional area and wall venting. This approach appeared to offer no advantage over the use of a constant flow area and a constant vent area in the reduction of attenuation time; however, the variable area venting approach may prove useful when seeking to minimize the length of the attenuator.

Vented Duct Performance

A three-dimensional plotting routine was developed to display the output of the FACTS code. Examples of these types of plots are shown in Figs. 6 and 7 where pressure and temperature are plotted as a function of position and time. In Fig. 6 in particular, one can distinguish all the prominent compressive wave structures that are indicated in the conventional x-t diagram of Fig. 3. One can see directly not only the paths of the dominant waves, but also their relative strengths.

The job of the acoustic attenuator will be to reduce the strength of the major shocks (A and B of Fig. 6), the reflected shock (AB), and the contact surface reflections; i.e., to weaken waves B_2 and C which appear in the laser cavity region.

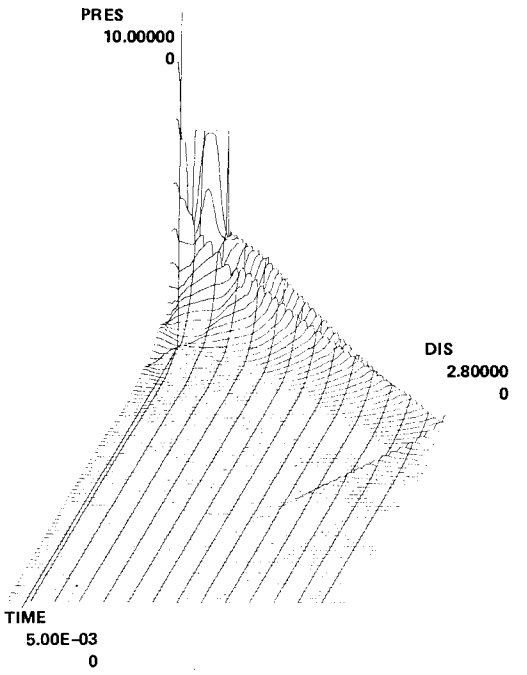

Fig. 9a Vented duct attenuator three-dimensional wave diagram for the first pulse.

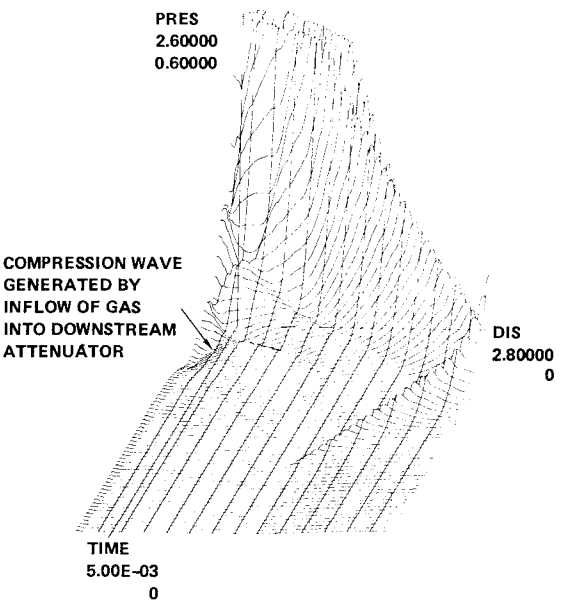

Fig. 9b Detailed three-dimensional pressure wave diagram with the vertical scale reduced from that of Fig. 9a.

Some typical FACTS code calculated pressure distributions are shown in Figs. 9 through 14 for the case of a 30-cm cavity with upstream and downstream venting (see Fig. 8 for venting geometry details). The first set of figures (Figs. 9-11) represents the results of a single pulse. Figures 12-14 represent the combined effect of the first and second pulses for a device pulsed at 200 pulses/s. (To perform the two-pulse calculation, cavity pressures and temperatures are reset to their initiation values after the first 5 ms.) These second-pulse results include the formation of a new shock that is reflected back into the laser cavity. This new shock is formed when a rarefaction wave generated by the second pulse interacts with the upstream contact surface of the first pulse.

If one compares Fig. 9a (vented duct) with Fig. 6 (unvented duct), one can see that the vents produce a significant at-

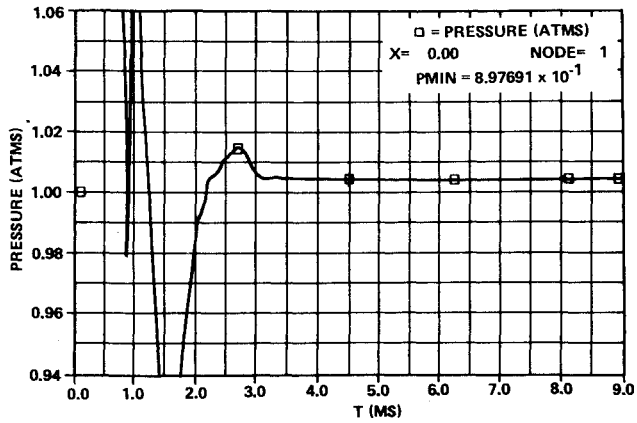

Fig. 10a Pressure history at the feed plate ($x = 0$) for the vented duct attenuator of Fig. 8.

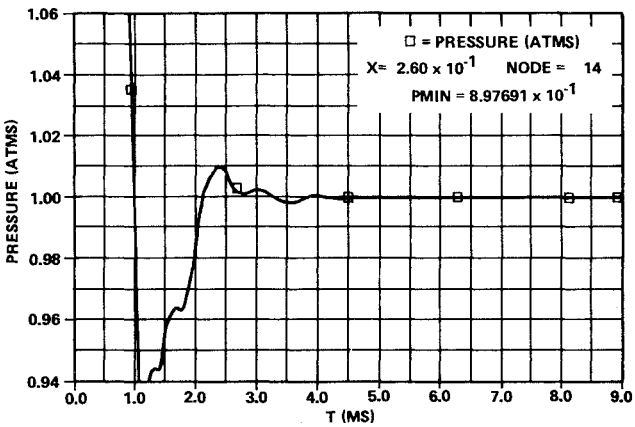

Fig. 10b Pressure history at the center of the cavity ($x = 26$ cm) for the vented duct attenuator of Fig. 8.

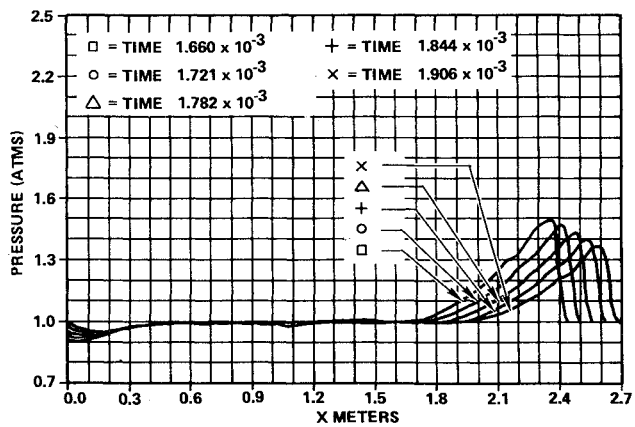

Fig. 11a Pressure-distance curves for the vented duct attenuator of Fig. 8 in the 1.6-1.9 ms after-initiation time interval for the first pulse.

tenuation of the dominant waves. Immediately evident is the major attenuation of the shock reflected from the downstream end of the duct. The contact surface reflections have not been eliminated by the venting system, but they have been significantly weakened.

A more detailed look at the late-time, low-amplitude venting process is seen in Fig. 9b. One prominent new compression wave seen in the vented case is the wave generated near the start of the downstream vent region. This wave is produced by an inflow into the duct, at a time when the local duct and cavity pressures have dropped below 1 atm. This late-time compression, which raises the cavity back to very near 1 atm, is clearly evident in Figs. 10a and 10b.

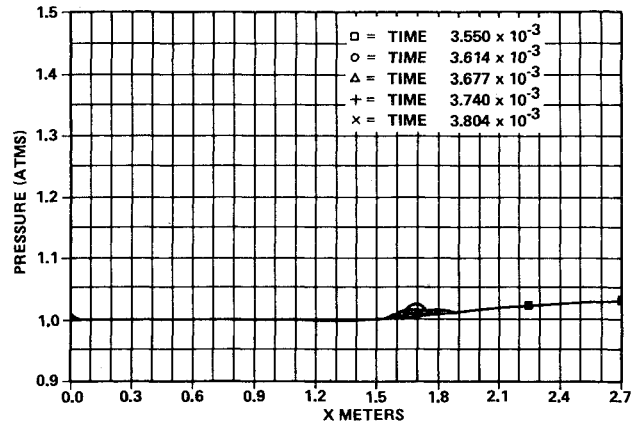

Fig. 11b Pressure-distance curves for the vented duct attenuator of Fig. 8 in the 3.5-3.8 ms after-initiation time interval for the first pulse.

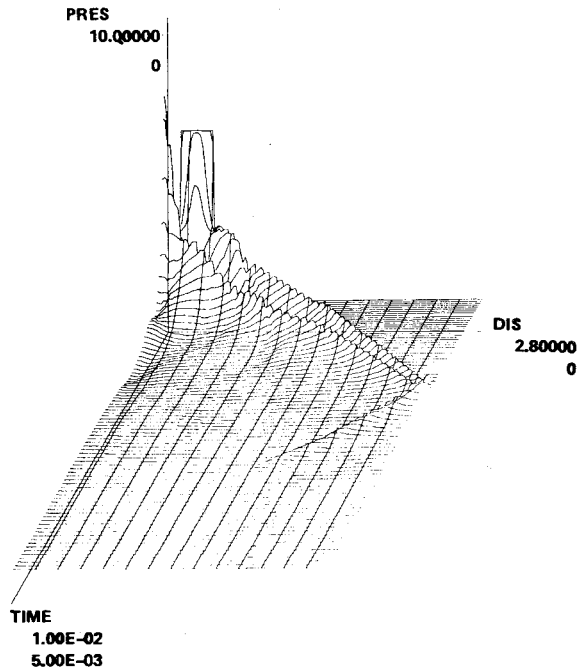

Fig. 12a Three-dimensional wave diagram of the second pulse ($5 < t < 10$ ms time interval) for the vented duct attenuator.

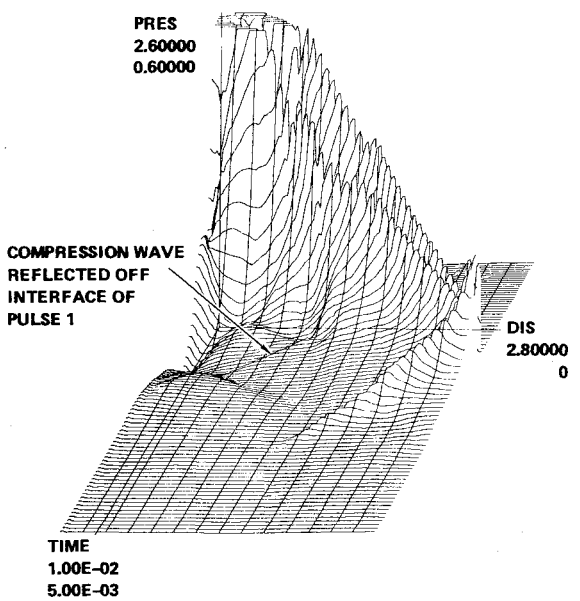

Fig. 12b Detailed three-dimensional wave diagram with reduced pressure scale of the second pulse for the vented duct attenuator.

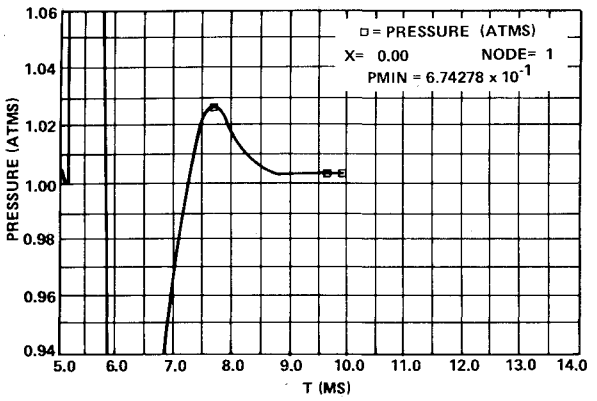

Fig. 13 Pressure history at the feed plate for the second pulse with the vented duct attenuator.

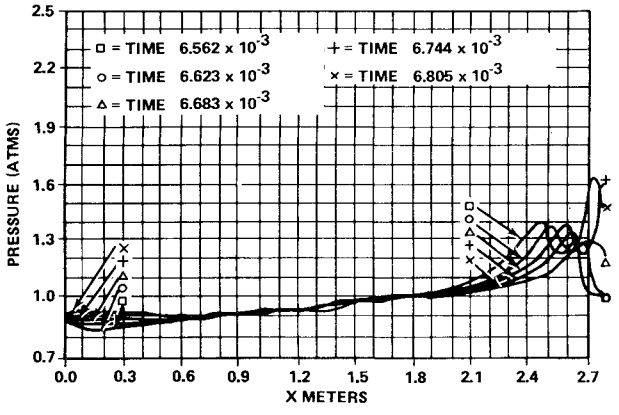

Fig. 14 Pressure-distance curves for the second pulse of the vented duct attenuator during the 6.56-6.80 ms time interval.

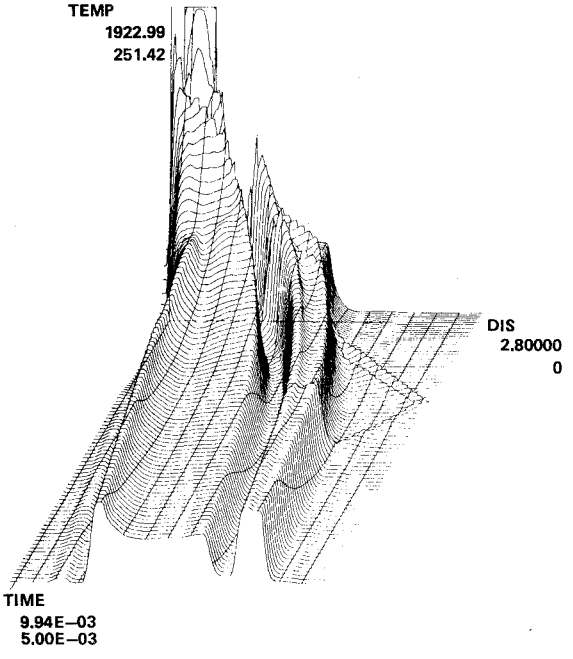

Fig. 15 Three-dimensional temperature diagram of the second pulse ($5 < t < 10$ ms time interval) for the vented duct attenuator.

Figures 10a and 10b show the pressure time history at individual points in the flow duct [at $x = 0$ (upstream feed plate) and $x = 26$ cm (center of cavity)]. These two figures principally show the effect, after 1 ms, of a rarefaction sent from the venting region, which drops the cavity pressure below 1 atm followed by a compression (from the same region), which

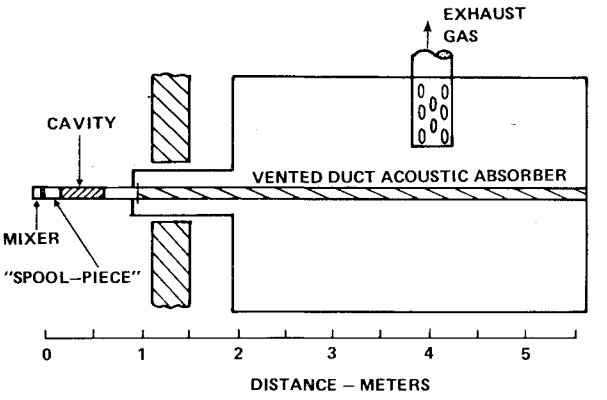

Fig. 16 Schematic of device used in flameout studies.

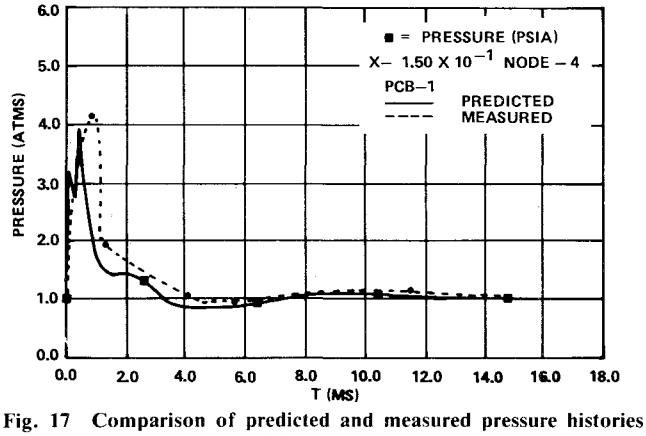

Fig. 17 Comparison of predicted and measured pressure histories just upstream of laser cavity (piezoelectric pressure transducer).

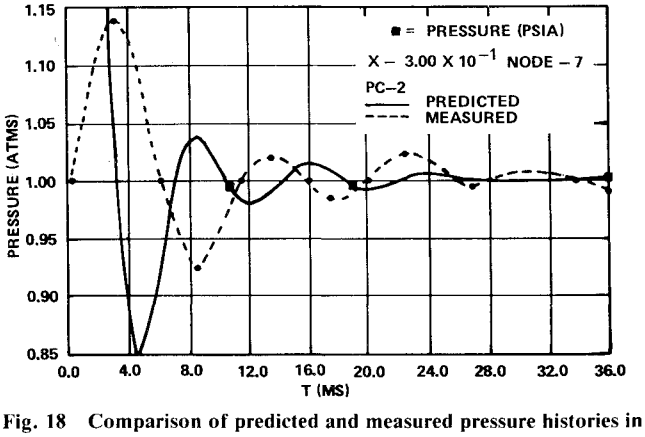

Fig. 18 Comparison of predicted and measured pressure histories in center of cavity (strain gage pressure transducer).

raises the pressure to slightly above ambient. The final equilibration process can also be seen in the pressure-distance plots of Figs. 11a and 11b.

Figures 12-15 ($t = 5$-10 ms) illustrate the effects of the dominant waves of a second pulse interacting with the residual contact surface from the first pulse (see the temperature plot of Fig. 15).

The basic overall pressure attenuation history of the second pulse is the same as that of the first pulse; however, some of the details of the weaker waves are different. For example, as noted in Fig. 12b, a weak compression wave reflecting off the interface of the first pulse arrives back into the cavity region just before final pressure equilibrium is achieved. For the configuration of this example, the calculated attenuation or damping time (to reach $\Delta P/P \sim 10^{-3}$) is seen in Figs. 10 and 13 to be between 3 and 4 ms. The above calculations indicate that acoustic suppression on very short time scales is possible.

Comparisons of Theory and Experiment

The FACTS code was used to develop the preliminary design of the vented duct suppressor for the flameout tests performed during 1976. The tests were performed to study the flameout characteristics of a 50 pps D_2/F_2 flashlamp-initiated laser system. A series of calculations was made to determine the optimum amount of venting and the optimum vented length. The basic design is shown in Fig. 16. The device included a 60-m/s purge flow. No upstream venting was included in the attenuator design.

The code calculations indicated that, after a period of 8-10 ms, a pressure oscillation was set up in the cavity which could be characterized as a quarter wave. According to the code, the strength of this quarter wave appears to be sensitive to the injection rate of the purge gas.

A comparison is made in Figs. 17 and 18 between predicted and measured pressure time histories. A pressure-time piezoelectric transducer trace covering the full pressure range ($0.8 \text{ atm} < P < 5 \text{ atm}$) is shown in Fig. 17 (15 cm downstream of the screen pack). Fairly good agreement between theory and data is seen in Fig. 17 both in the overall magnitude of the early-time shock overpressures and in the qualitative behavior of the late-time pressure history.

More sensitive measurements of the cavity pressure ($x = 30$ cm) for $t > 4$ ms are shown plotted in Fig. 18, where strain gage transducer data are compared with predictions from the FACTS code. The strain gage pressure transducer does not have the frequency response to follow the early-time pressure history, but it can follow the late-time ($t > 4$ ms) pressure history. The quarter-wave phenomenon is clearly seen in the data. The experimental pressure oscillations are out of phase with the theoretical oscillations, and the over-pressure magnitude is about a factor of 2 greater than predicted. The magnitude and phase of the cavity pressure oscillations were influenced to some degree by the presence of the outer cylindrical manifold, used to help vent off the exhaust gases. It appears that pressure disturbances in the outer manifold need to be treated in any future modeling and design efforts on the vented duct system.

VI. Conclusions

This paper has analyzed the one-dimensional aspects of pressure wave suppression in pulsed chemical lasers. A finite-difference code was developed for evaluating various attenuation schemes. Several methods of attenuation were analyzed, including porous flow through absorbers, ducts lined with absorbing material, acoustic horns (impedance matching), and vented ducts. Of the attenuation concepts considered, the vented duct concept offered the most promise of achieving the desired attenuation.

Acknowledgment

The analytical work, code development, and shock tube tests were supported by TRW Systems and Energy Group IR&D. The flameout tests were supported by the Defense Advanced Projects Research Agency (DARPA) and the Naval Research Laboratories (NRL). S. Searles of NRL served as government technical monitor.

References

[1]Scheidegger, A. E., "Hydrodynamics in Porous Media," *Encyclopedia of Physics*, Vol. VIII/2, Springer-Verlag, Berlin, 1963, Chap. C.

[2]Schlichting, H., *Boundary Layer Theory*, 4th ed., McGraw-Hill, New York, 1960, pp. 303-305, and pp. 492-495.

[3]Boris, J. P. and Books, D. L., "Flux-Corrected Transport-I. SHASTA, A Fluid Transport Algorithm that Works," *Journal of Computational Physics*, Vol. 2, Jan. 1973, pp. 38-69.

[4]Book, D. L., Boris, J. P., and Hain, K., "Generalizations of the Flux-Corrected Transport Technique, Naval Research Laboratory, Washington, D.C., NRL Memorandum Rept. No. 3021, April 1975.